Article

Cell Reports

An Excitatory Neural Assembly Encodes Short-Term Memory in the Prefrontal Cortex

Graphical Abstract

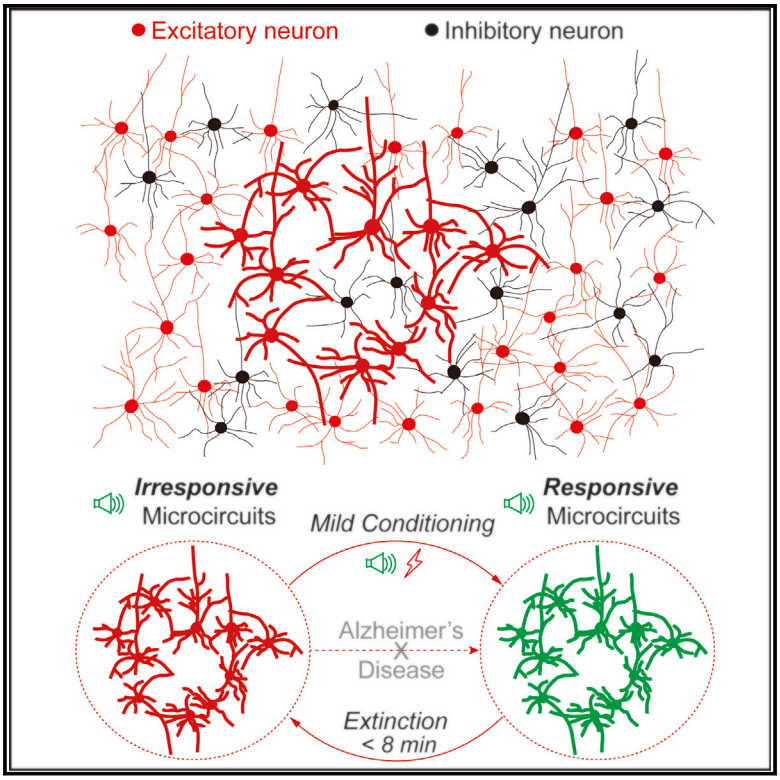

Authors

Yonglu Tian, Chaojuan Yang, Yaxuan Cui, ..., Zilong Qiu, Xiang-Yao Li, Chen Zhang

Correspondence

zqiu@ion.ac.cn (Z.Q.), lixiangy@zju.edu.cn (X.-Y.L.), ch.zhang@pku.edu.cn (C.Z.)

In Brief

Using two-photon imaging on behaving mice, Tian et al. discover a functional coding mechanism that relies on the emergent behavior of a functionally defined neuronal assembly to encode short-term memory. They further demonstrate that this coding mechanism is absent in an animal model of Alzheimer's disease (AD).

Highlights

- Two-photon imaging enables the monitoring of neural activities on behaving animals
- A neuronal subpopulation in the mPFC that exhibited emergent properties encodes STM
- These neuronal subpopulations exclusively comprise excitatory neurons
- This STM coding mechanism is absent in an animal model of AD

Tian et al., 2018, Cell Reports *22*, 1734–1744
February 13, 2018
https://doi.org/10.1016/j.celrep.2018.01.050

CellPress

OPEN ACCESS
CellPress

Cell Reports
Article

An Excitatory Neural Assembly Encodes Short-Term Memory in the Prefrontal Cortex

Yonglu Tian,[1,2,15] Chaojuan Yang,[1,15] Yaxuan Cui,[1,15] Feng Su,[1,3,15] Yongjie Wang,[4,5,15] Yangzhen Wang,[1,6,15] Peijiang Yuan,[3] Shujiang Shang,[1] Hao Li,[7,8] Jizong Zhao,[7,8] Desheng Zhu,[1] Shiming Tang,[1] Peng Cao,[9] Yunbo Liu,[10] Xunli Wang,[11] Liecheng Wang,[12] Wenbo Zeng,[13] Haifei Jiang,[13] Fei Zhao,[13] Minhua Luo,[13] Wei Xiong,[6] Zilong Qiu,[14,*] Xiang-Yao Li,[5,*] and Chen Zhang[1,16,*]

[1]State Key Laboratory of Membrane Biology, PKU-IDG/McGovern Institute for Brain Research, School of Life Sciences and Key Laboratory for Neuroscience, Ministry of Education/National Health and Family Planning Commission, Peking University, Beijing 100191, China
[2]Peking-Tsinghua Center for Life Sciences, Academy for Advanced Interdisciplinary Studies, Peking University, Beijing 100871, China
[3]School of Mechanical Engineering and Automation, Beihang University, Beijing 100191, China
[4]Center for Mitochondrial Biology and Medicine, and Key Laboratory of Biomedical Information Engineering of the Ministry of Education, School of Life Science and Technology, Frontier Institute of Science and Technology, Xi'an Jiaotong University, Xi'an, Shaanxi Province 710049, China
[5]Department of Physiology, Institute of Neuroscience and Collaborative Innovation Center for Brain Science, School of Medicine, Zhejiang University, Hangzhou, Zhejiang Province 310058, China
[6]School of Medicine, School of Life Sciences, Tsinghua University, Beijing 100084, China
[7]Department of Neurosurgery, Beijing Tiantan Hospital, Capital Medical University, Beijing 100050, China
[8]China National Clinical Research Center for Neurological Diseases, Beijing 100050, China
[9]State Key Laboratory of Brain and Cognitive Sciences, Institute of Biophysics, Chinese Academy of Sciences (CAS), Beijing 100101, China
[10]Institute of Laboratory Animal Science, Peking Union Medical College/Chinese Academy of Medical Science, Beijing 100021, China
[11]Laboratory Animal Center, Fujian University of Tradition Chinese Medicine, Fuzhou, Fujian Province 350122, China
[12]Department of Physiology, Anhui Medical University, Hefei, Anhui Province 230032, China
[13]State Key Laboratory of Virology, CAS Center for Excellence in Brain Science and Intelligence Technology, Wuhan Institute of Virology, CAS, Wuhan, Hubei Province 430071, China
[14]CAS Key Laboratory of Primate Neurobiology, Institute of Neuroscience, CAS, Shanghai 200031, China
[15]These authors contributed equally
[16]Lead Contact
*Correspondence: zqiu@ion.ac.cn (Z.Q.), lixiangy@zju.edu.cn (X.-Y.L.), ch.zhang@pku.edu.cn (C.Z.)
https://doi.org/10.1016/j.celrep.2018.01.050

SUMMARY

Short-term memory (STM) is crucial for animals to hold information for a small period of time. Persistent or recurrent neural activity, together with neural oscillations, is known to encode the STM at the cellular level. However, the coding mechanisms at the microcircuitry level remain a mystery. Here, we performed two-photon imaging on behaving mice to monitor the activity of neuronal microcircuitry. We discovered a neuronal subpopulation in the medial prefrontal cortex (mPFC) that exhibited emergent properties in a context-dependent manner underlying a STM-like behavior paradigm. These neuronal subpopulations exclusively comprise excitatory neurons and mainly represent a group of neurons with stronger functional connections. Microcircuitry plasticity was maintained for minutes and was absent in an animal model of Alzheimer's disease (AD). Thus, these results point to a functional coding mechanism that relies on the emergent behavior of a functionally defined neuronal assembly to encode STM.

INTRODUCTION

Short-term memory (STM) is the capacity to hold information in the brain in an active, readily accessible state for a brief period of time, typically from seconds to minutes (Jonides et al., 2008; Richardson, 2007). Deficits in STM are associated with the pathogenesis of many psychiatric disorders, including Alzheimer's disease (AD) and posttraumatic stress disorder (PTSD). For example, familial AD patients exhibit deficits in verbal memory about two years before an official diagnosis of AD (Fox et al., 1998), and sporadic AD patients show significant impairment in veridical recall in a semantically associated word list learning task (MacDuffie et al., 2012). People with PTSD show worse non-verbal STM on the Benton visual retention test, possibly because of dysfunction in the hippocampal (Emdad and Sönder-gaard, 2006).

Unlike long-term memory that depends on protein synthesis (Davis and Squire, 1984; Jarome and Helmstetter, 2014), STM seems to depend on firing patterns at the cellular level (Fuster and Alexander, 1971; Goldman-Rakic, 1995; Miller et al., 1996; Rawley and Constantinidis, 2009; Wang, 2001). The encoding mechanism of STM has been most studied in the context of working memory, which involves both STM and a central executive module. Extensive studies have shown that a persistent

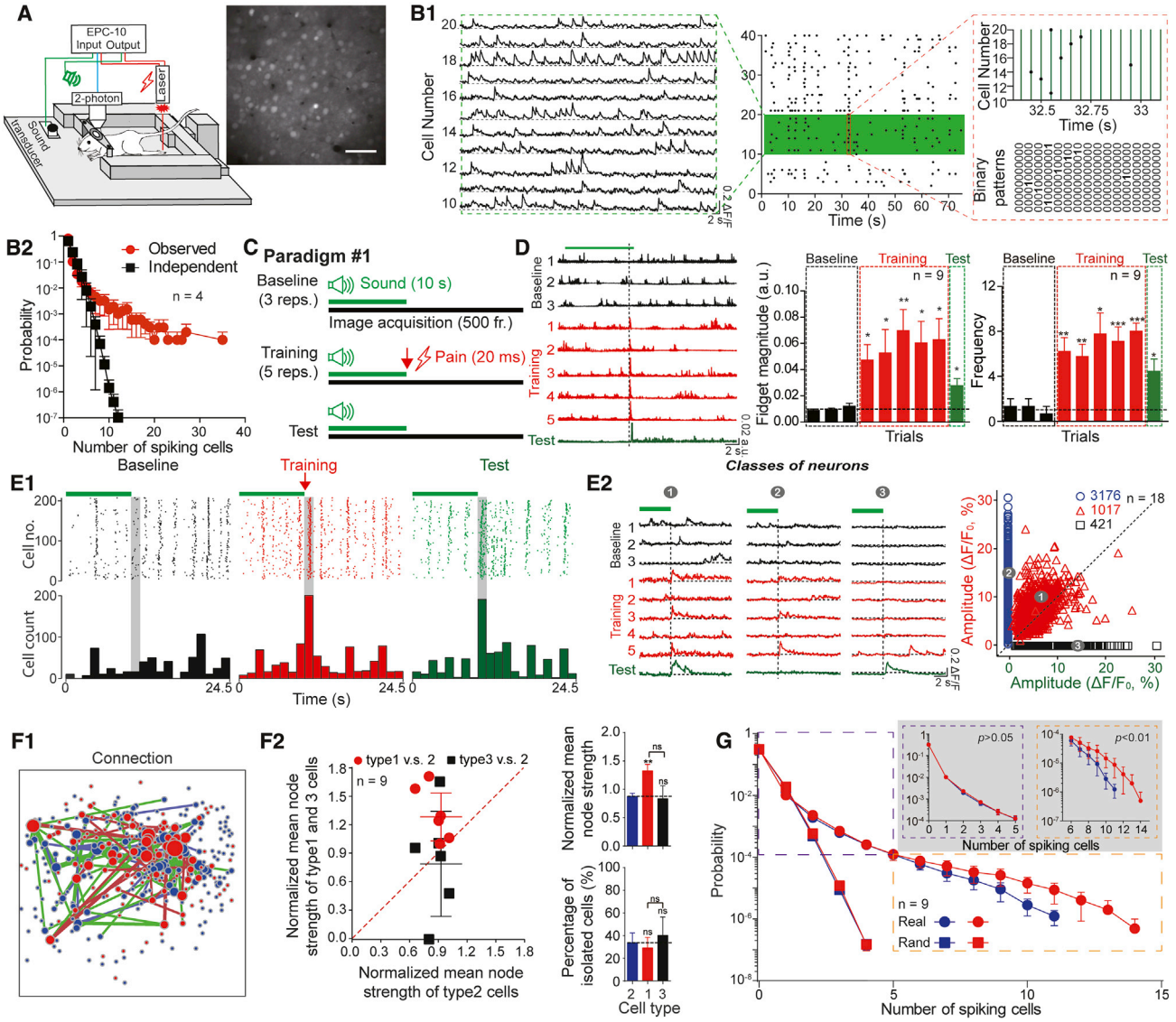

Figure 1. Behavior of a PFC Microcircuitry Underlying a STM-like Training Paradigm

(A) Schematic diagram of the experiment setup for imaging the neuronal activities with a two-photon microscope from a head-fixed behaving mouse. A piezoelectric sensor was placed under the forepaws of the mouse to record fidgeting movements. The EPC-10 amplifier controlled the sound cue, pain delivery, and image acquisition through transister-transister logic (TTL) signals. The inset figure shows a typical field of L2/3 neurons stained with OGB-1. Scale bar, 50 μm.

(B1) Left panel: representative traces of the simultaneous responses of 40 neurons in the PFC microcircuitry. Middle panel: a segment of the simultaneous responses of 40 neurons in the PFC microcircuitry; each dot represents the time of a transient peak. Right panel: discretization of the transient spike trains into a binary pattern of the red-boxed area in the middle panel; each string (bottom panel) describes the activity pattern of the neurons at a given point in time.

(B2) The probability distribution of synchronous spiking events from the spontaneous recording of PFC neurons (red circle). The plot of the probability distribution at the chance level was calculated as the averaged probability from randomly shuffling the recorded spike trains 50 times (black square, n = 4).

(C) Training paradigm.

(D) Behavior test using the paradigm in (C). Left panel: illustrative traces show the changes in fidgeting that underlie paradigm #1. Middle panel: magnitude of fidgeting 0.5 s after the end of the 10-s sound cue was averaged. Right panel: average frequency of fidgeting 0.5 s after the end of the 10-s sound cue (n = 9).

(E1) Responses of the PFC neurons from a C57BL/6 wild-type mouse during stimulation, as depicted in (C). Top: representative raster plot showing the activity events of all recorded neurons during the trials. Bottom: a histogram of the number of activity events (bin size, 1.25 s). The gray bar indicates the 1.25-s time window after the end of the sound stimulus during the baseline, training, and test periods.

(E2) Example traces of calcium signals (left) and a scatterplot of the spike amplitude (right) of the three functional groups of PFC neurons (n = 18).

(F1) Complex network model of a microcircuitry. Each node denotes a neuron located at its real position in a two-photon image. Red, blue, and black nodes denote groups 1, 2, and 3 neurons, respectively. Red, blue, and gray lines denote the intra-class links between red-red, blue-blue, and black-black neuron pairs, respectively. Green lines denote the inter-class links between red-blue, red-black, and blue-black neuron pairs. The thickness of the line positively correlates to its weight. The size of the node positively correlates to its strength.

(legend continued on next page)

firing in the neurons in a recurrently connected neural network underlies STM storage. This "persistent firing" phenomenon has been identified in many brain regions, including the prefrontal cortex (PFC) (Fuster and Alexander, 1971), parietal (Gnadt and Andersen, 1988), and inferotemporal cortex (Fuster and Jervey, 1981) but with significant trial-to-trial variability (Shafi et al., 2007). Furthermore, the duration of the elevated firing in the neurons correlates well with the maintenance of the STM in animals, making it an attractive model to represent the storage of STM. Other cellular mechanisms for STM, such as changes in the intrinsic properties in individual neurons (Dash et al., 2007; Egorov et al., 2002; Hasselmo et al., 2000; Sidiropoulou et al., 2009), also have been proposed. Membrane depolarization in deep-layer PFC pyramidal neurons that is induced by persistent activity has been shown to occur without recurrent synaptic activity (Sidiropoulou et al., 2009). Short-term Hebbian synaptic plasticity, such as short-term potentiation (STP), has been experimentally characterized in hippocampal neurons and proposed as a candidate mechanism for STM (Erickson et al., 2010).

Though the cellular mechanism for STM coding has been extensively examined in multiple brain areas, including the PFC and hippocampus, spatial and temporal coding of STM at the microcircuitry level in either the sensory cortex or the PFC remains elusive, partially because of the lack of a direct visualization of microcircuitry activity during STM tasks. In the current study, we monitored microcircuit activities using two-photon calcium imaging in the PFCs and sensory cortexes in awake mice and found that an excitatory neural assembly in the PFC encodes STM. We further demonstrate that this STM-related plasticity was impaired in an animal model of AD.

RESULTS

Properties of the PFC Microcircuitry Underlying a STM-like Training Paradigm

We used a two-photon *in vivo* imaging technique to measure the activities of neuronal networks at the single-neuron resolution in a 517.77 × 517.77 μm area in the brains of head-fixed awake mice (Figure 1A). Oregon Green BAPTA-1-AM (OGB-1, a calcium dye, Life Technologies) was injected into the brain to label individual neurons (Figure 1A, inset). To examine whether neurons in the mPFC microcircuitry formed a functionally interconnected circuit, we calculated the correlations of neuronal activities among multiple neurons by recording spontaneous activities for 122.5 s. The activities were all digitized as a binary sequence: either firing a calcium spike (Ca^{2+} spike) (1) or not (0) at one given time point. The correlation probability (CP (n)) was calculated as the probability of n neurons firing Ca^{2+} spike synchronously at one time point (Figure 1B1). When choosing a microcircuitry comprising 40 mPFC neurons, the pairwise correlation CP (2) was rather weak (0.104 ± 0.014) and not significantly higher from that of the same pair of neurons after each cell's spike train was randomized (0.236 ± 0.058). However, when examining the high order correlation by plotting the CP curve with an increasing n, the actual CP curve drastically deviated from the curve that was calculated from the independent model (Figure 1B2). For example, the average CP (10) calculated from the actual data was 2×10^{-3}, whereas the expected probability when all 10 neurons were assumed to be independent from each other was 1.4×10^{-6}. These results clearly demonstrate that neurons in the mPFC microcircuitry had become functionally interconnected with each other.

We trained the mice to make an association between a neutral cue (a 10-s presentation of sound at 50 dB, 6 kHz) and a weak noxious pain stimulus induced by a laser (20 ms, 7 W), and then we had the mice actively maintain this STM until the test trial (Figure 1C, paradigm #1). The learning process consisted of five trials that paired the presentation of the neutral cue with the pain stimulation, followed by a 2-min inter-trial interval. Note that the laser-induced pain stimulation was applied right after the termination of the cue. A piezoelectric sensor positioned under the forepaws of the head-fixed mouse monitored the animal's fine movements. The mice showed no obvious fidgeting movements during the baseline recordings (amplitude: 0.011 ± 0.001 a.u., frequency: 1.000 ± 0.333 Hz) when compared to the pain stimulus during the learning period (0.059 ± 0.013 a.u., $p = 0.006$; frequency: 6.880 ± 0.487 Hz, $p < 0.001$; pairwise t test). In the test trial, the animal showed apparent fidgeting behavior to only the cue stimulation (0.021 ± 0.003 a.u., $p = 0.01$; frequency: 4.000 ± 1.075 Hz, $p = 0.023$; compared to the baseline period, pairwise t test), which shows that the animal held the information obtained during the learning period (Figure 1D).

Next, we used the same training paradigm to monitor the activities of the mPFC microcircuitry. Initially, the neurons showed no baseline response to the sound cue alone and produced synchronous Ca^{2+} spikes in response to the laser-induced pain stimulation during the associative period (Figure 1E1). These data indicate that the mPFC microcircuitry normally responds to acute skin pain, but not to the sound stimulation (neutral cue) that was applied in this study. However, in the test trial after associative learning, a significant portion of the mPFC neurons fired Ca^{2+} spikes in response to the cue presentation without pain stimulation (Figure 1E1, right). This was consistent with the behavior results (Figure 1D), which showed that the mice could predict the upcoming pain stimulation by actively holding the cue-pain association during the 10-min association period. Statistically, the proportions of neurons that fired Ca^{2+} spikes within a time window of 0.5 s after the termination of the cue presentation during the baseline, learning, and test trials were 6.8% ± 1.2%, 31.8% ± 3.8%, and 18.9% ± 3.6%, respectively (Figure S1A). Furthermore, the

(F2) Assessment criteria for groups 1, 2, and 3 neurons in complex network models. Left: the plot of the normalized mean node strength of groups 1 and 3 neurons against the normalized mean node strength of group 2 neurons. The dotted red line denotes a vertical ordinate equal to the horizontal ordinate. Top right: summary graph of the normalized mean node strength of a cell. Bottom right: percentage of isolated cells for the three kinds of neurons (n = 9).
(G) Probability distribution of synchronous spiking events in training that record group 1 neurons (red circle) and group 2 neurons (blue circle). Twenty neurons were randomly chosen to calculate the probability distribution for groups 1 and 2 neurons. Red square (group 1) and blue square (group 2): the distribution of synchronous events for the same neurons after shuffling each cell's spike train to eliminate all correlations. The insert panels show the low-order correlation (left) and high-order correlation (right) for groups 1 and 2 neurons (n = 9). Error bar represents SEM.

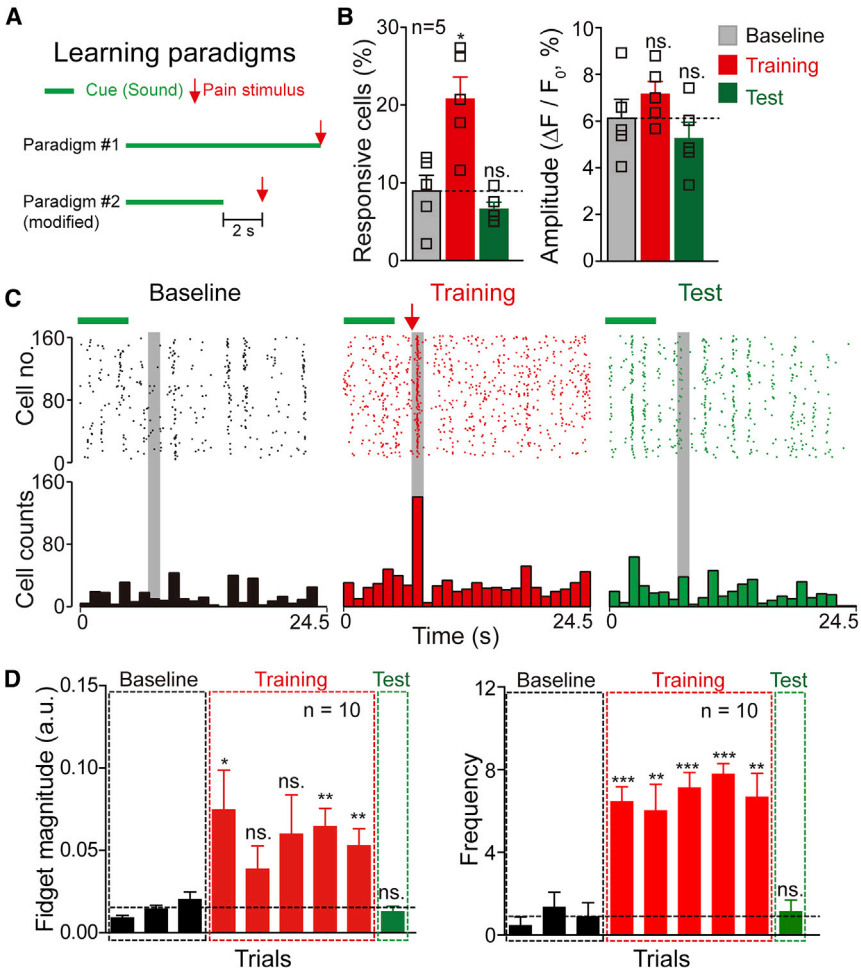

Figure 2. The Training Behavior of the Neuronal Microcircuitry Is Context Specific

(A) Training paradigm. Figure 1C shows paradigm #1. In paradigm #2, a 5-s sound cue was applied immediately after image acquisition began (three times) for the baseline recording. After a 2-s gap, following the 5-s sound cue, a 20-ms heat-based pain was delivered to establish associative learning (five times). One sound cue (test) was applied to monitor the neuronal activity in the local circuit.

(B) Average percentages (left) and amplitude (right) of the positive cells in the prefrontal cortex (PFC) in the baseline, training, and test periods (n = 5).

(C) Responses of the PFC neurons from a C57BL/6 wild-type mouse when paradigm #2 was applied.

(D) Behavior test using paradigm #2. The magnitude (left) and frequency (right) of fidgeting was averaged 0.5 s after the end of the 2-s gap, which followed the 5-s sound cue (n = 10). Error bar represents SEM.

distribution of the Ca^{2+} spike delays relative to the termination of the sound cue in the test trials showed two Gaussian distributions with peaks at 0.11 and 0.40 s, whereas the learning trials had a single Gaussian distribution with a peak at 0.31 s, and the baseline period showed a random distribution (Figure S1B). These results reinforce the notion that the appearance of the time-correlated Ca^{2+} spikes in the test trial was a specific consequence of learning during the information-holding (learning) process rather than a spontaneous activity.

Plotting the Ca^{2+} spike amplitudes in the learning trials versus the test trials revealed three functional groups of mPFC neurons: group 1, where the neurons changed their responsiveness from cue-negative to cue-positive after a brief training; group 2, where the neurons remained cue-negative after the training; and Group 3, where the neurons did not respond to pain but became responsive to the cue after learning (Figure 1E2). The proportions of neurons in the mPFC in groups 1, 2, and 3 were 16.5% ± 3.5%, 63.1% ± 3.6%, and 2.4% ± 0.6%, respectively. It is worth noting that 14.7% ± 2.0% of the mPFC neurons in our study remained silent (unresponsive) across all conditions and were not included in the statistics. Because the precise location of each neuron was known, we examined the connectivity strength among the three different groups of neurons. The average Ca^{2+} spike frequencies for the neurons in groups 1, 2, and 3 were essentially indistinguishable (0.057 ± 0.040 Hz, 0.052 ± 0.050 Hz, and 0.054 ± 0.060 Hz, respectively). Two neurons were considered to be functionally connected when there was at least one synchronous Ca^{2+} spike during the 24.5-s recording of spontaneous activity. When plotting the neurons in circles using diameters proportional to the total strength of the connections, the neurons in group 1 exhibited much stronger connectivity compared to the other two groups (Figure 1F1). Statistically, the neurons in group 1 were 44.76% more functionally connected neurons compared to the neurons in group 2 (Figure 1F2, unpaired t test). We also calculated the CP curves for the neurons in groups 1 and 2 to examine the high-order correlation in the mPFC microcircuitry. When n was in the range of 5–15, the CP curves for the neurons in group 1 were significantly higher than those in group 2, but they were indistinguishable when n was in the range of 1–5 (Figure 1G). These results demonstrate that the neurons in the mPFC microcircuitry formed different neuronal assemblies with distinct functional connectivity features, but they were physically indistinguishable.

The Training Behavior of the Neuronal Microcircuitry Is Context Specific

For animals to learn a cause-and-effect relationship, the precise coupling between the cue and stimulus must be finely controlled (Molet and Miller, 2014). Therefore, we modified paradigm #1 by inserting a 2-s interval between the cue and stimulus (Figure 2A, paradigm #2), which resembled a trace-conditioning paradigm (Bangasser et al., 2006; Connor and Gould, 2016). Although the stimulus effectively induced Ca^{2+} spikes when the laser fired, the mPFC neurons failed to fire synchronous Ca^{2+} spikes in the test trial (Figures 2B and 2C). Behaviorally, the pain stimulations induced apparent fidgeting movements

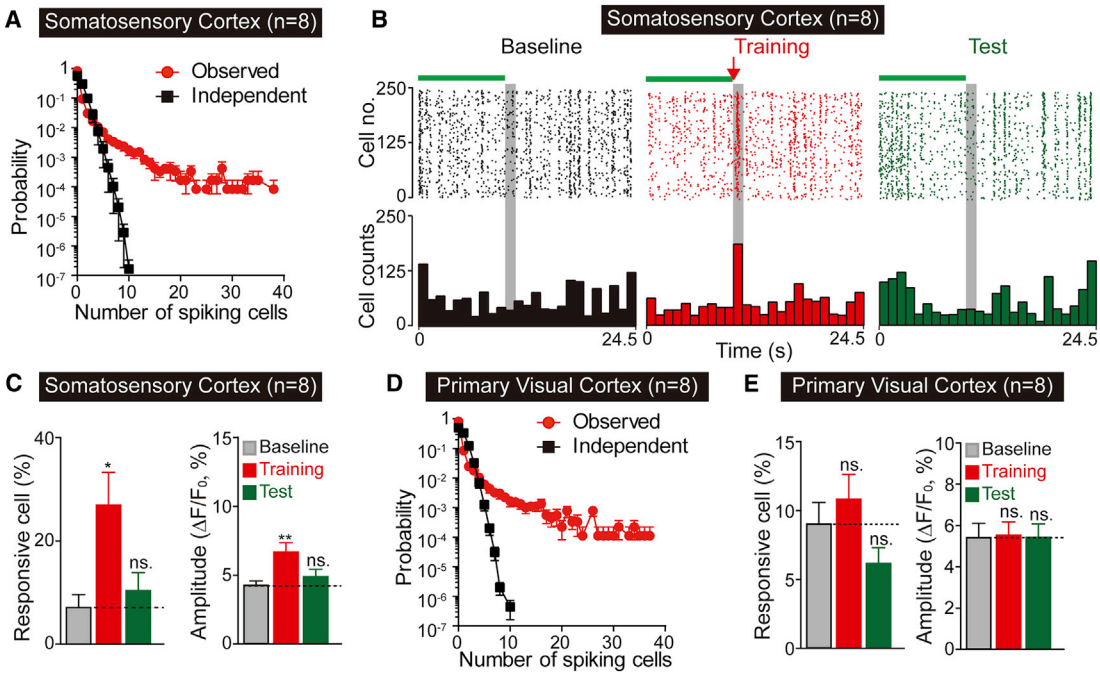

Figure 3. The Training Behavior of the Neuronal Microcircuitry Is Region Specific in the Brain

(A) Probability distribution of synchronous spiking events during the spontaneous recording of SSC neurons (red circle). Black square: the distribution of synchronous events for the same neurons after shuffling each cell's spike train to eliminate all correlations (n = 8).

(B) Responses of neurons in the SSC from a C57BL/6 wild-type mouse when paradigm #1 was applied (n = 8).

(C) Average percentages (left) and amplitude (right) of responsive cells in the somatosensory cortex in the baseline, training, and test periods (n = 8).

(D) Probability distribution of synchronous spiking events during the spontaneous recording of primary visual cortex neurons (red circle). Black square: the distribution of synchronous events for the same neurons after shuffling each cell's spike train to eliminate all correlations (n = 8).

(E) Average percentages (left) and amplitude (right) of responsive cells in the primary visual cortex in the baseline, training, and test periods (n = 8). Error bar represents SEM.

(amplitude: 0.054 ± 0.009 a.u., p = 0.001; frequency: 6.800 ± 0.632 Hz, p < 0.001; pairwise t test), while the cue-alone stimulus failed to induce significant fidgeting movement (amplitude: 0.012 ± 0.002 a.u., p = 0.54; frequency: 1.112 ± 0.588 Hz, p = 0.763; pairwise t test) compared to the baseline period (amplitude: 0.014 ± 0.002 a.u., frequency: 0.889 ± 0.458 Hz) (Figure 2D). These results indicate that the presentation of STM in the PFC critically depends on the context in which a cue and a stimulus are presented.

The Training Behavior of the Neuronal Microcircuitry Is Region Specific

To test whether the sensory cortex was involved in storing of the cue information received during the training in paradigm #1, we examined the microcircuitry plasticity in the somatosensory cortex (SSC), which is a sensory cortex involved in the perception of multiple types of sensations, including pain and pressure, from the body (Bushnell et al., 1999; Feldman and Brecht, 2005; Haggard, 2006). The primary visual cortex (V1), an unrelated brain area involved in perceiving and processing visual information, was also included as a control experiment. The comparison of CP curves versus those at the chance level demonstrates highly connected microcircuitry in both the SSC and V1 cortex (Figures 3A and 3D), similar to those observed in the mPFC (Figure 1B2). Neurons in the SSC were consistently activated following the pain stimulation and did not hold the cue-stimulus information reflected as lacking cue-elicited responses after learning (Figures 3B and 3C). These observations indicate that the sensory cortex, specifically the SSC in paradigm #1, did not store information from the cue-stimulus training. This also rules out the possibility that the cue activated the mPFC neurons in the test period as a result of direct cue-induced activation in the SSC. Furthermore, the stimulus-cue pairing failed to change the microcircuitry responsiveness in the V1 cortex (Figures 3E and S2). To test whether mPFC neurons are more connected to each other than the SSC or V1 region of the cortex, we further compared synchronized activity in these brain regions. By randomly selecting a microcircuitry of 40 neurons in these three regions, the averaged CP curve of the mPFC is significantly above those from the SSC and V1 regions (Figure S3), suggesting that the neurons in the mPFC are indeed more connected by recurrent pathways.

The Training Behavior of the Neuronal Microcircuitry Is Transient and Subject to Rapid Extinction

To test whether this type of information-holding process in the mPFC is subjected to extinction, we monitored the decline of newly gained responsiveness when multiple test trials were applied. We found that the mPFC microcircuitry maintained its responsiveness to the cue for a couple of test trials before becoming unresponsive (Figure 4A, also known as

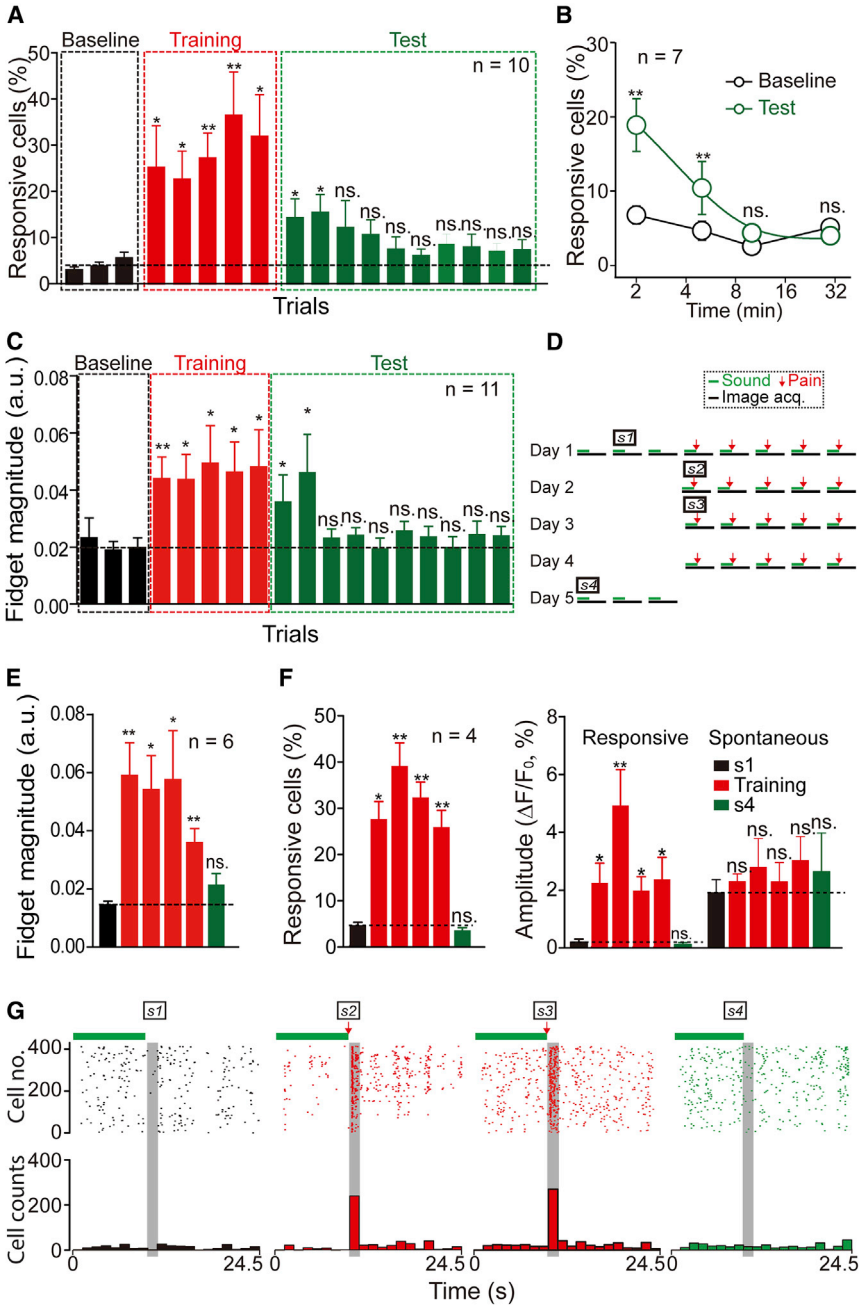

Figure 4. The Training Behavior of the Neuronal Microcircuitry Is Transient and Subject to Rapid Extinction

(A) Percentage of responsive cells in the baseline, training, and test trials. The test trials were repeated 10 times with an inter-trial interval of 2 min (n = 10).

(B) Percentage of responsive cells in the baseline (black) and test (green) periods. The test trials were conducted 2, 5, 10, and 30 min after the last training trial (n = 7).

(C) Behavior test using a slightly modified version of the paradigm in Figure 1C. The test trials were repeated 10 times with an inter-trial interval of 2 min. The magnitude of fidgeting 0.5 s after the end of the 10-s sound cue was averaged (n = 11).

(D) The training paradigm for long-term associative training. On day 1, a 10-s sound cue was immediately applied after the start of image acquisition for the baseline recording (three times). A 20-ms heat-based pain was immediately delivered after the 10-s sound cue to establish associative learning (five times). On days 2, 3, and 4, the associative learning procedure was repeated five times on each day. On day 5, the sound cue alone was applied three times, during which fidgeting movements and neuronal activity in the local circuit were monitored. Four representative stages were chosen: (s1) baseline on day 1, (s2) associative learning on day 2, (s3) associative learning on day 3, and (s4) sound cue alone stimulus on day 5.

(E) Behavior test using the paradigm in (D). The magnitude of fidgeting 0.5 s after the end of the 10-s sound cue was averaged (n = 6).

(F) Left: average baseline percentage of positive cells on day 1 (black); training on days 1, 2, 3, and 4 (red); and test trials on day 5 (green). Right: average amplitude of positive cells during the baseline, training, and test periods in a responsive manner (i.e., events were counted during the responsive window) and spontaneous manner (i.e., events were counted during the entire recording time, except for the responsive window, n = 4).

(G) The responses of the PFC neurons from a *Thy1*-GCaMP3 mouse when the stimulation depicted in (D) was applied. The four illustrative situations shown here are those depicted in (D). Top: raster plot showing activity events of all neurons during the trials. Bottom: a histogram of the activity events (bin size, 1.25 s). The gray bar indicates the 1.25-s time window after the end of the sound stimulus. Error bar represents SEM.

"reverse training"). The animals showed similar behavior patterns (Figures 4C and S4, pairwise t test). We then tested how long the learned information would hold without disturbance by monitoring the microcircuitry activity with increasing intervals between the last learning trial and test trial. The results showed that the mPFC microcircuitry maintained its responsiveness to the cue for up to 5 min and switched back to a cue-unresponsive status after a period of 10 min or longer (Figure 4B, pairwise t test), which is consistent with the notion that the observed circuit plasticity reflects a form of STM.

To confirm that the association in paradigm #1 is a weak stimulus for inducing STM, but not long-term memory, we repeated this training paradigm once every day for 4 consecutive days using transgenic mice that expressed GCaMP3 (Chen et al., 2012) in order to conduct long-term *in vivo* imaging. We applied the cue stimulus on the fifth day (Figure 4D). The behavior data show that the cue stimulus on the last day did not induce significantly enhanced fidgeting movement (amplitude: 0.023 ± 0.003 a.u.) compared to the baseline period (amplitude: 0.015 ± 0.002 a.u., p = 0.109; pairwise t test) (Figure 4E). Similarly, we found

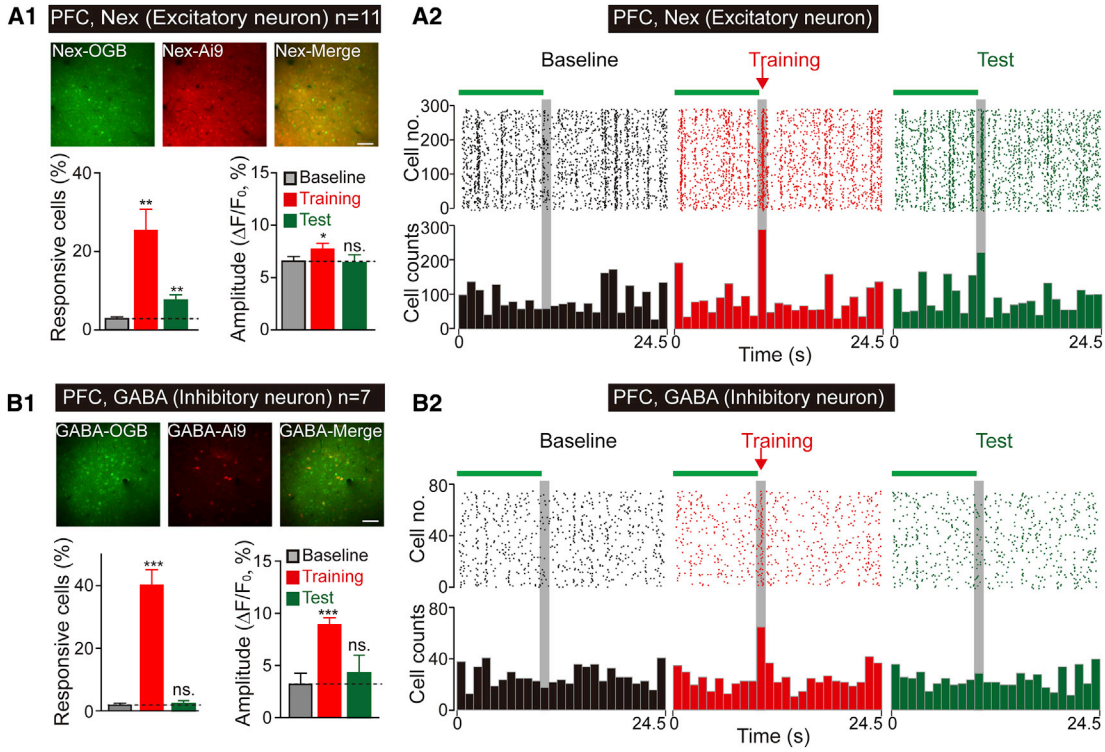

Figure 5. Behavior of Excitatory and Inhibitory Neurons of the PFC Microcircuitry Underlying the Sound and Pain Training Paradigm

(A1) Top: excitatory neurons labeled with td-tomato and stained with OGB-1 simultaneously. Scale bar, 25 μm. Bottom: average percentages (left) and amplitude (right) of the positive cells of excitatory neurons in PFC during the baseline, training, and test periods (n = 11).

(A2) Responses of excitatory PFC neurons from a Nex-Ai9 mouse during the stimulation depicted in Figure 1C. Top: raster plot showing the activity events of all the neurons during the trials. Bottom: a histogram of the number of activity events (bin size, 1.25 s). The gray bar indicates the 1.25-s time window after the end of the sound stimulus during the baseline, training, and test periods.

(B1) Top: inhibitory neurons labeled with td-tomato and stained with OGB-1 simultaneously. Scale bar, 25 μm. Bottom: average percentages (left) and amplitude (right) of the positive cells of inhibitory neurons in the PFC during the baseline, training, and test periods (n = 7).

(B2) Responses of inhibitory PFC neurons from a GABA-Ai9 mouse during the stimulation depicted in Figure 1C. Top: raster plot showing the activity events of all neurons during the trials. Bottom: a histogram of the number of activity events (bin size, 1.25 s). The gray bar indicates the 1.25-s time window after the end of the sound stimulus during the baseline, training, and test periods. Error bar represents SEM.

that the percentage of cue-responsive cells did not increase on day 5 compared to before learning (Figure 4F; 4.58% ± 0.43% versus 4.20% ± 1.15%, pairwise t test) although the pain stimulus elicited comparable neuronal responses on every training day (Figure 4G). These results indicate that the activated status of the mPFC microcircuitry underlying paradigm #1 encodes the STM but is not capable of self-perpetuation as long-term memory.

mPFC Microcircuitry Plasticity Is Mediated by Excitatory Neurons in a Context-Specific Manner

To test the neuronal-type specificity of the information-holding neurons in the mPFC, we crossed *NEX*- and *GABA-Cre* transgenic mice with *Ai9* indicator mice to label the excitatory and inhibitory neurons, respectively. We found that the excitatory neurons, which were red-labeled with a td-tomato fluorescent marker in the *NEX-Ai9* mice, exhibited cue-evoked Ca^{2+} spikes in the test trial (Figure 5A, pairwise t test); however, the *GABAergic* neurons remained unresponsive to the cue, which is reflected as an undistinguished percentage of cue-responsive neurons before and after learning (Figure 5B, pairwise t test). Thus, mPFC microcircuitry plasticity is mediated by excitatory neurons in a context-specific manner.

STM-Related Microcircuitry Plasticity in mPFC Is Absent in *5XFAD* Mice

The performance of human learning depends on STM (Edwards et al., 2016; van Iterson and de Jong, 2018; Murrihy et al., 2017; Purser et al., 2012). Therefore, we examined the mPFC microcircuitry plasticity in *5XFAD* transgenic mice, which are animal models of AD and are characterized with severe learning and memory deficits (Oakley et al., 2006). We found that the emergence of cue-responsiveness in neurons in the mPFC was completely absent in the *5XFAD* transgenic mice, while it was apparent in wild-type mice (Figures 6A and 6B, pairwise t test). This difference was not due to general mPFC dysfunction in the *5XFAD* transgenic mice because these animals showed normal spontaneous mPFC activity (Figure S5) and a normal response to the pain stimulus (Figure 6B, pairwise t test). Consistently, the behavioral data show that the cue stimulus did not

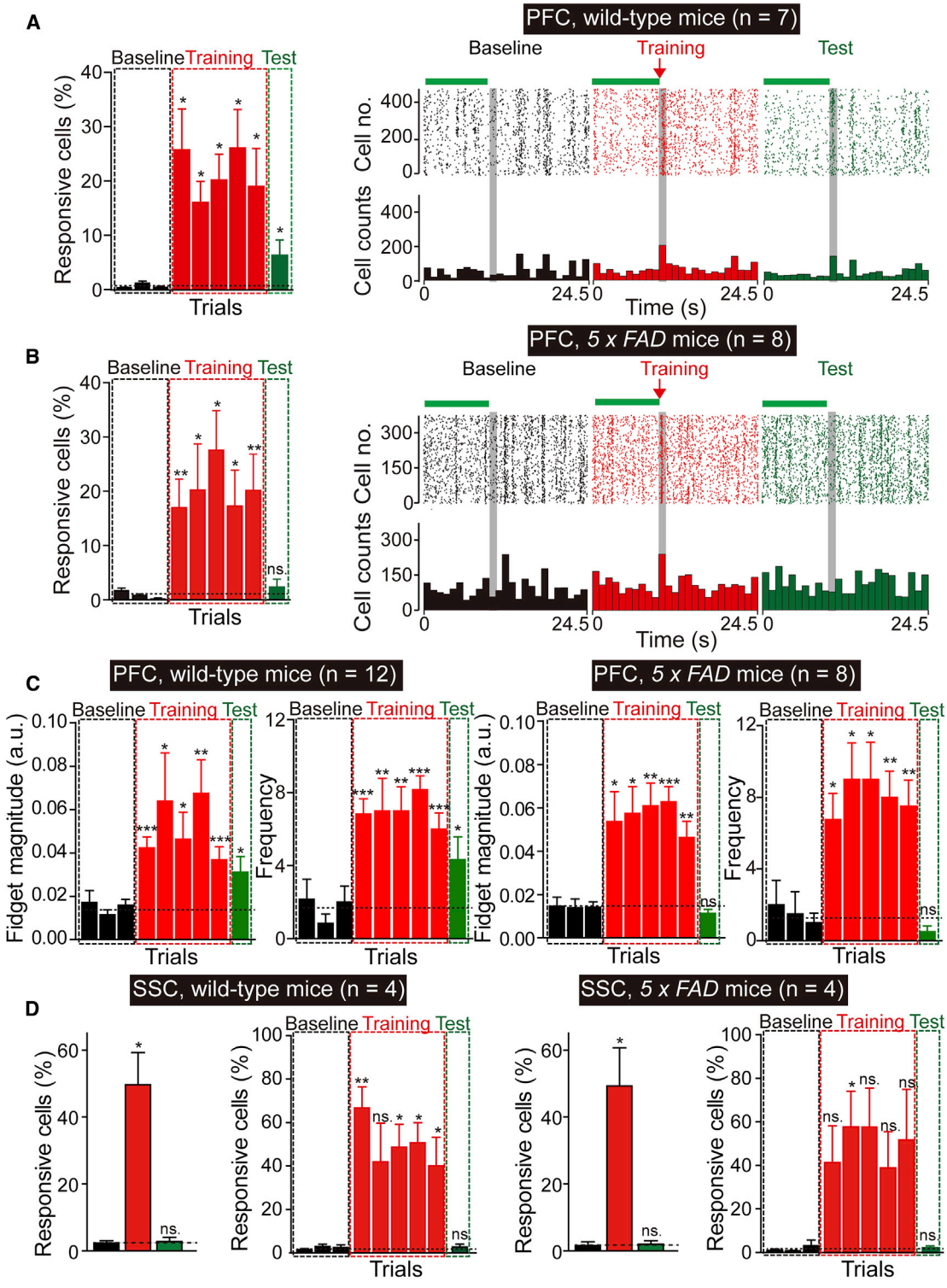

Figure 6. The Emergence of Cue-Responsive Neurons Is Absent in *5XFAD* Mice

(A) Left: percentage of responsive cells in the PFC of wild-type mice during the baseline, training, and test trials. Right: responses of PFC neurons from a wild-type mouse when paradigm #1 was applied (n = 7).

(B) Left: percentage of responsive cells in the PFC of *5XFAD* mice during the baseline, training, and test trials. Right: responses of PFC neurons from a *5XFAD* mice when paradigm #1 was applied (n = 8).

(legend continued on next page)

induce significantly enhanced fidgeting movement (amplitude: 0.021 ± 0.004 a.u., frequency: 0.500 ± 0.327) compared to the baseline period (amplitude: 0.014 ± 0.001 a.u., p = 0.120; frequency: 1.500 ± 0.546, p = 0.230; pairwise t test) in the *5XFAD* transgenic mice (Figure 6C). Furthermore, we found that learning-dependent plasticity was absent in the SSC of the *5XFAD* transgenic mice (Figure 6D, pairwise t test), which is in line with similar observations on the SSC in the wild-type mice (Figures 3B and 3C). It is important to note that the pain stimulus induced almost similar responses (49.28% ± 2.27%) in the *5XFAD* transgenic mice compared to the SSC in the wild-type mice (49.65% ± 1.91%), which excludes the possibility of insensitivity to pain in the *5XFAD* transgenic mice. Therefore, the specific absence of mPFC plasticity underlying paradigm #1 in the *5XFAD* transgenic mice was not because of differences in overall mPFC activity or SSC responsiveness. Thus, these results reveal the presence of a microcircuitry mechanism that underlies the impaired STM in an AD animal model.

DISCUSSION

Overall, we have identified a type of microcircuitry plasticity in the PFC that resembles the behavioral phenomenon of STM in several ways: (1) both require active storage of information during the learning period, and (2) both are modulated by training protocols and diminish as time passes. By switching the circuit property from a cue-unresponsive state to a cue-responsive state, the identified circuit holds the newly learned information. The circuit plasticity in the mPFC exhibits Hebbian-like behavior. When two inputs excite the microcircuitry in a precise temporal sequence, the microcircuitry becomes ''inter-associated'' or ''auto-associated.'' The emergent state lasts for only a short time; the circuit switches back to its original state after approximately 5 min.

Interestingly, this type of STM does not rely on sustained activity during the memory-holding period. This is different from what happens during a working memory task, which also involves STM storage (Fuster and Alexander, 1971; Goldman-Rakic, 1995; Miller et al., 1996; Rawley and Constantinidis, 2009; Wang, 2001). Our results show that the transient formation of cell assemblies in the mPFC that keep an association over a few minutes serves as an alternative mechanism for STM expression. Though calcium imaging provides superior spatial resolution, the limitation in sensitivity makes it difficult to reveal neuronal activity at a single action-potential (AP) resolution. Thus, our results cannot rule out the possibility that other mechanisms, such as spike timing or patterning, could also contribute to the coding of STM at the microcircuit level. Interestingly, a similar form of short-term Hebbian synaptic plasticity, NMDAR-dependent associative STP that subject to activity-dependent decay, was previously reported in hippocampal neurons underlying relative weak stimulation (not sufficient to induce LTP) (Erickson et al., 2010; Volianskis et al., 2015). Conceptually, both phenomena involve associative synaptic or microcircuit modifications without persistent firing, implying that such mechanisms may contribute to the attractor state in the learning and memory process.

The neurons in the microcircuitry are functionally interconnected with each other, which is reflected in the plots of the CP curves from the mPFC, SSC, and V1 (Figures 1B2, 3A, and 3D, respectively). Furthermore, the responses of the microcircuitry to a given stimulus (i.e., the pain stimulus in this study) follow the uncertainty principle, meaning it is difficult to decode the stimulus simply from the firing frequencies of hundreds of neurons, even with precise spatial information. Given the identical pain stimulus that was applied to the mice over five rounds, only 0.9% ± 0.4% of the mPFC neurons and 2.3% ± 1.3% of the SSC neurons responded to the stimulation every time. The average firing probability of a Ca^{2+} spike in these two areas was 16.67% ± 4.85% and 16.29% ± 5.13%, respectively. This uncertainty resembles the fact that transmitter release at single excitatory or inhibitory synapses is also a probability event (Hessler et al., 1993; Rosenmund et al., 1993). Though there was no apparent pattern associated with the location or firing probability of a Ca^{2+} spike in the cue-responsive and cue-unresponsive neurons in the mPFC, we provide clear evidence that excitatory neurons form functional correlated entities based on pairwise correlations in a neural population (Figures 1 and 5). This is important in terms of the functional connectivity diagram at the microcircuit level, meaning that emergent properties could be mediated by a defined neuronal entity rather than a group of randomly selected neurons from an upper-level circuit. One limitation of the current study is that we only measured the fidget behavior on awake head-fixed mice together with two-photon imaging, thus providing only the most limited of behavioral measurements of conditioning. Further development of other associated behavioral paradigms will be crucial as a means of interpreting what the altered mPFC means functionally, e.g., motor-related versus cognitive activity.

The coding mechanism underlying the connection between the uncertain behavior of individual neurons, the defined entity holding the cue information in a microcircuitry, and the predictable macroscopic biological effects are fascinating topics that merit further investigation, especially considering that the overall input and output to the microcircuitry in each trial were basically consistent (in other words, the mice felt pain every time the pain stimulus was applied). Furthermore, the absence of STM-related microcircuitry plasticity in the mPFC in an AD animal model (*5XFAD* transgenic mice) is consistent with the STM disabilities reported in AD patients (MacDuffie et al., 2012; Querfurth and LaFerla, 2010; Scheltens et al., 2016; Selkoe, 2002). Therefore, an investigation into the details of the mechanism that underlies STM-like microcircuitry plasticity in the mPFC would likely provide an explanation for AD pathology from a circuit point of view.

(C) Behavior test of wild-type and *5XFAD* mice. The magnitude and frequency of fidgeting was averaged out at 0.5 s after the end of the 2-s gap following the 5-s sound cue (wild-type: n = 12, *5XFAD*: n = 8).
(D) Percentage of responsive cells in the SSC of wild-type mice and *5XFAD* mice during the baseline, training, and test periods (wild-type: n = 4, *5XFAD*: n = 4). Error bar represents SEM.

EXPERIMENTAL PROCEDURES

Animals

The current study was conducted at an Association for Assessment and Accreditation of Laboratory Animal Care (AAALAC)-approved Animal Facility at Peking University Laboratory Animal Center (LAC-PKU), which has been previously described (Tian et al., 2017; Zeng et al., 2017). Wild-type C57BL/6 mice (males, aged 2– 3 months) were purchased from Vital River Laboratories (Beijing, China). 5XFAD transgenic mice (males, aged 2-3 months) were purchased from the Jackson Laboratory (Bar Harbor, ME, USA, strain no. 008730). *Thy1*-GCaMP3 transgenic mice (males, aged 2– 3 months) were used in the long-term experiment.

In Vivo Two-Photon Imaging

For two-photon imaging, the fluorescence transient in the cortical neurons was monitored using a commercial two-photon microscope equipped with a tunable ultrafast laser at 920 nm. The imaging data were analyzed using ImageJ and MATLAB. Weighted functional networks were generated from the recordings of the spontaneous activity.

Statistical Analysis

All statistical analyses were performed using GraphPad Prism software (Jiang et al., 2017; Wei et al., 2016). The data are presented as the mean ± SEM. Statistical analyses were performed using Student's t tests, and statistical significance was set at $^*p < 0.05$.

Further details can be found in the Supplemental Experimental Procedures.

SUPPLEMENTAL INFORMATION

Supplemental Information includes Supplemental Experimental Procedures and six figures and can be found with this article online at https://doi.org/10.1016/j.celrep.2018.01.050.

ACKNOWLEDGMENTS

We thank Drs. Thomas C. Südhof and Lu Chen for beneficial discussions and critical comments on the manuscript. This work was supported by grants from the National Basic Research Program of China (2017YFA0105201 and 2014CB942804), the National Science Foundation of China (31670842 and 61375085), Beijing Institute of Collaborative Innovation (15I-15-BJ), Beijing Municipal Science & Technology Commission (Z161100002616021 and Z161100000216154), and SLS-Qidong Innovation Fund and the Seeding Grant for Medicine and Life Sciences of Peking University (2014-MB-11).

AUTHOR CONTRIBUTIONS

Y.T., C.Y., Y.C., F.S., Yongjie W., and Yangzhen W. carried out the experiments; P.Y., S.S., H.L., J.Z., D.Z., S.T., P.C., Y.L., X.W., L.W., W.Z., H.J., F.Z., M.L., W.X., Z.Q., X.-Y.L., and C.Z. contributed to the planning of the work; and C.Z. wrote the paper.

DECLARATION OF INTERESTS

The authors declare no competing interests.

Received: July 12, 2017
Revised: December 1, 2017
Accepted: January 16, 2018
Published: February 13, 2018

REFERENCES

Bangasser, D.A., Waxler, D.E., Santollo, J., and Shors, T.J. (2006). Trace conditioning and the hippocampus: the importance of contiguity. J. Neurosci. *26*, 8702–8706.

Bushnell, M.C., Duncan, G.H., Hofbauer, R.K., Ha, B., Chen, J.I., and Carrier, B. (1999). Pain perception: is there a role for primary somatosensory cortex? Proc. Natl. Acad. Sci. USA *96*, 7705–7709.

Chen, Q., Cichon, J., Wang, W., Qiu, L., Lee, S.J.R., Campbell, N.R., Destefino, N., Goard, M.J., Fu, Z., Yasuda, R., et al. (2012). Imaging neural activity using Thy1-GCaMP transgenic mice. Neuron *76*, 297–308.

Connor, D.A., and Gould, T.J. (2016). The role of working memory and declarative memory in trace conditioning. Neurobiol. Learn. Mem. *134* (*Pt B*), 193–209.

Dash, P.K., Moore, A.N., Kobori, N., and Runyan, J.D. (2007). Molecular activity underlying working memory. Learn. Mem. *14*, 554–563.

Davis, H.P., and Squire, L.R. (1984). Protein synthesis and memory: a review. Psychol. Bull. *96*, 518–559.

Edwards, L., Aitkenhead, L., and Langdon, D. (2016). The contribution of short-term memory capacity to reading ability in adolescents with cochlear implants. Int. J. Pediatr. Otorhinolaryngol. *90*, 37–42.

Egorov, A.V., Hamam, B.N., Fransén, E., Hasselmo, M.E., and Alonso, A.A. (2002). Graded persistent activity in entorhinal cortex neurons. Nature *420*, 173–178.

Emdad, R., and Söndergaard, H.P. (2006). General intelligence and short-term memory impairments in post traumatic stress disorder patients. J. Ment. Health *15*, 205–216.

Erickson, M.A., Maramara, L.A., and Lisman, J. (2010). A single brief burst induces GluR1-dependent associative short-term potentiation: a potential mechanism for short-term memory. J. Cogn. Neurosci. *22*, 2530–2540.

Feldman, D.E., and Brecht, M. (2005). Map plasticity in somatosensory cortex. Science *310*, 810–815.

Fox, N.C., Warrington, E.K., Seiffer, A.L., Agnew, S.K., and Rossor, M.N. (1998). Presymptomatic cognitive deficits in individuals at risk of familial Alzheimer's disease. A longitudinal prospective study. Brain *121*, 1631–1639.

Fuster, J.M., and Alexander, G.E. (1971). Neuron activity related to short-term memory. Science *173*, 652–654.

Fuster, J.M., and Jervey, J.P. (1981). Inferotemporal neurons distinguish and retain behaviorally relevant features of visual stimuli. Science *212*, 952–955.

Gnadt, J.W., and Andersen, R.A. (1988). Memory related motor planning activity in posterior parietal cortex of macaque. Exp. Brain Res. *70*, 216–220.

Goldman-Rakic, P.S. (1995). Cellular basis of working memory. Neuron *14*, 477–485.

Haggard, P. (2006). Sensory neuroscience: from skin to object in the somatosensory cortex. Curr. Biol. *16*, R884–R886.

Hasselmo, M.E., Fransen, E., Dickson, C., and Alonso, A.A. (2000). Computational modeling of entorhinal cortex. Ann. N Y Acad. Sci. *911*, 418–446.

Hessler, N.A., Shirke, A.M., and Malinow, R. (1993). The probability of transmitter release at a mammalian central synapse. Nature *366*, 569–572.

Jarome, T.J., and Helmstetter, F.J. (2014). Protein degradation and protein synthesis in long-term memory formation. Front. Mol. Neurosci. *7*, 61.

Jiang, W., Wei, M., Liu, M., Pan, Y., Cao, D., Yang, X., and Zhang, C. (2017). Identification of protein tyrosine phosphatase receptor type O (PTPRO) as a synaptic adhesion molecule that promotes synapse formation. J. Neurosci. *37*, 9828–9843.

Jonides, J., Lewis, R.L., Nee, D.E., Lustig, C.A., Berman, M.G., and Moore, K.S. (2008). The mind and brain of short-term memory. Annu. Rev. Psychol. *59*, 193–224.

MacDuffie, K.E., Atkins, A.S., Flegal, K.E., Clark, C.M., and Reuter-Lorenz, P.A. (2012). Memory distortion in Alzheimer's disease: deficient monitoring of short- and long-term memory. Neuropsychology *26*, 509–516.

Miller, E.K., Erickson, C.A., and Desimone, R. (1996). Neural mechanisms of visual working memory in prefrontal cortex of the macaque. J. Neurosci. *16*, 5154–5167.

Molet, M., and Miller, R.R. (2014). Timing: an attribute of associative learning. Behav. Processes *101*, 4–14.

Murrihy, C., Bailey, M., and Roodenburg, J. (2017). Psychomotor ability and short-term memory, and reading and mathematics achievement in children. Arch. Clin. Neuropsychol. *32*, 618–630.

Oakley, H., Cole, S.L., Logan, S., Maus, E., Shao, P., Craft, J., Guillozet-Bongaarts, A., Ohno, M., Disterhoft, J., Van Eldik, L., et al. (2006). Intraneuronal beta-amyloid aggregates, neurodegeneration, and neuron loss in transgenic mice with five familial Alzheimer's disease mutations: potential factors in amyloid plaque formation. J. Neurosci. *26*, 10129–10140.

Purser, H.R.M., Farran, E.K., Courbois, Y., Lemahieu, A., Mellier, D., Sockeel, P., and Blades, M. (2012). Short-term memory, executive control, and children's route learning. J. Exp. Child Psychol. *113*, 273–285.

Querfurth, H.W., and LaFerla, F.M. (2010). Alzheimer's disease. N. Engl. J. Med. *362*, 329–344.

Rawley, J.B., and Constantinidis, C. (2009). Neural correlates of learning and working memory in the primate posterior parietal cortex. Neurobiol. Learn. Mem. *91*, 129–138.

Richardson, J.T.E. (2007). Measures of short-term memory: a historical review. Cortex *43*, 635–650.

Rosenmund, C., Clements, J.D., and Westbrook, G.L. (1993). Nonuniform probability of glutamate release at a hippocampal synapse. Science *262*, 754–757.

Scheltens, P., Blennow, K., Breteler, M.M.B., de Strooper, B., Frisoni, G.B., Salloway, S., and Van der Flier, W.M. (2016). Alzheimer's disease. Lancet *388*, 505–517.

Selkoe, D.J. (2002). Alzheimer's disease is a synaptic failure. Science *298*, 789–791.

Shafi, M., Zhou, Y., Quintana, J., Chow, C., Fuster, J., and Bodner, M. (2007). Variability in neuronal activity in primate cortex during working memory tasks. Neuroscience *146*, 1082–1108.

Sidiropoulou, K., Lu, F.M., Fowler, M.A., Xiao, R., Phillips, C., Ozkan, E.D., Zhu, M.X., White, F.J., and Cooper, D.C. (2009). Dopamine modulates an mGluR5-mediated depolarization underlying prefrontal persistent activity. Nat. Neurosci. *12*, 190–199.

Tian, Y., Yang, C., Shang, S., Cai, Y., Deng, X., Zhang, J., Shao, F., Zhu, D., Liu, Y., Chen, G., et al. (2017). Loss of FMRP impaired hippocampal long-term plasticity and spatial learning in rats. Front. Mol. Neurosci. *10*, 269.

van Iterson, L., and de Jong, P.F. (2018). Development of verbal short-term memory and working memory in children with epilepsy: Developmental delay and impact of time-related variables. A cross-sectional study. Epilepsy Behav. *78*, 166–174.

Volianskis, A., France, G., Jensen, M.S., Bortolotto, Z.A., Jane, D.E., and Collingridge, G.L. (2015). Long-term potentiation and the role of N-methyl-D-aspartate receptors. Brain Res. *1621*, 5–16.

Wang, X.J. (2001). Synaptic reverberation underlying mnemonic persistent activity. Trends Neurosci. *24*, 455–463.

Wei, M., Zhang, J., Jia, M., Yang, C., Pan, Y., Li, S., Luo, Y., Zheng, J., Ji, J., Chen, J., et al. (2016). α/β-hydrolase domain-containing 6 (ABHD6) negatively regulates the surface delivery and synaptic function of AMPA receptors. Proc. Natl. Acad. Sci. USA *113*, E2695–E2704.

Zeng, W.B., Jiang, H.F., Gang, Y.D., Song, Y.G., Shen, Z.Z., Yang, H., Dong, X., Tian, Y.L., Ni, R.J., Liu, Y., et al. (2017). Anterograde monosynaptic transneuronal tracers derived from herpes simplex virus 1 strain H129. Mol. Neurodegener. *12*, 38.